# MICROSATELLITE FORMATION FLYING USING PULSED PLASMA THRUSTER AND SOLAR SAILING AT EARTH MOON L4

**Junquan Li[*], Steve Greenland[†], Craig Clark[‡], and Mark A. Post[§]**

This paper presents a deep space formation flying mission using microsatellites with pulsed plasma thrusters and solar sails as propulsion systems. The circular restricted three body problem with consideration of solar gravitation was used as the equation of motion. Formation flying near Earth Moon triangular libration points uses short period trajectories as relative references. Simulation results using a nonaffine control strategy are provided to demonstrate the effectiveness of the proposed propulsion systems for formation flying near triangular libration points.

## INTRODUCTION

The libration points are the equilibrium solutions of the classical circular restricted three body problem (see Reference 1). Libration point missions can provide unobstructed views of deep space and celestial bodies (see Reference 2). Most libration point missions have been deployed at the Sun Earth L1 (ISEE-3, WIND, SOHO, ACE, TRIANA) or L2 points (MAP, WSO, PLANK, GAIA, JSWT, Constellation X) (see Reference 3). The reasons for choosing these points are based on the mission requirements, or avoidance of the higher costs and engineering challenges associated with travelling longer distances to reach the other libration points in the Sun Earth. The collinear libration point of the Earth Moon system is suitable for space based observation missions due to the fact that the Sun, Earth and Moon are always behind the spacecraft with half of the celestial sphere available at all times. Also, the thermal stability of this region is favorable for non-cryogenic missions such as visible light telescopes. The collinear points is far enough away from Earth to avoid the effects of the atmosphere and space debris and close enough to allow a constant communications geometry. The triangular libration points (L4 and L5) are the locations of small bodies in the solar system (see Reference 4). L4 and L5 of the Earth Moon system were considered for the use of space colonies (see Reference 5). Communication between the triangular points to the Earth or between two triangular points can form a space VLBI (very long baseline interferometry) array and can enhance the accuracy of astronomical observations. Missions to the triangular libration points in the Sun Earth Moon system and even other libration points in the Solar system will become feasible in the near future making use of the stable properties near the triangular libration points. With recent renewed efforts to return to the Moon, it is likely that these points will be used for lunar mission support purposes. In the circular restricted three body problem, motion about these points is bounded, making

[*]Marie Curie Experienced Researcher at ASTRONETII and Clyde Space Ltd, Unit 5B Skypark 5, Glasgow, G3 8JU, United Kingdom.
[†]Senior System Engineer, Clyde Space Ltd, Unit 5B Skypark 5, Glasgow, G3 8JU, United Kingdom.
[‡]CEO, Clyde Space Ltd, Unit 5B Skypark 5, Glasgow, G3 8JU, United Kingdom.
[§]Lecturer, Department of Design, Manufacture and Engineering Management, 75 Montrose St. Glasgow, G1 1XJ, United Kingdom.

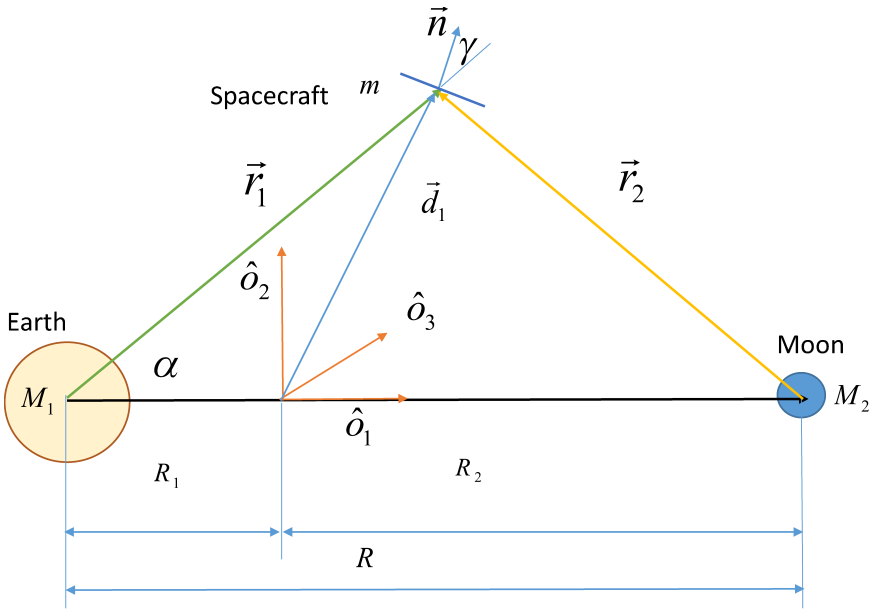


**Figure 1. Circular Restricted Three body Problem at System Barycenter**

them ideal locations for a variety of applications, including imaging interferometery and communication relay satellites. Satellite formation flying involves two or more spacecraft flying in particular configurations and working cooperatively towards achieving mission goals (see Reference 6). The successful miniaturization of satellite subsystems now makes microsatellites suitable candidates for many future missions (see Reference 7). Linear and nonlinear methods have been used for deep space spacecraft formation keeping and formation maneuvering (see References 8 and 9). In this paper, we present the mission concept of a 50 kg class microsatellite using a pulsed plasma thruster and solar sail with closed loop nonlinear control algorithms for microsatellite formation flying control near the Earth Moon L4 point. Simulation results for formation flying of this microsatellite with nonlinear control algorithms to maintain natural formation trajectories will be presented.

## EARTH MOON TRIANGULAR LIBRATION POINT ORBITS

### Circular Restricted Three Body Problem

In celestial mechanics, the motion of three point masses with the influence of their gravitational attraction, assuming the primary and secondary body are on circular orbits, is known as the circular restricted three body problem (see Figure 1). The rotating coordinate frame has the origin in the barycenter of Earth and Moon (see Reference 10). The distance between Earth and Moon is $R$. The distances between Earth, Moon and the barycenter are $R_1$ and $R_2$. The distances between Earth, Moon and the spacecraft are $r_1$ and $r_2$. The mass of the Earth, Moon and Spacecraft are $M_1$, $M_2$, and $m$ respectively. By defining a reference frame that rotates with the primaries, it is possible to determine five equilibrium solutions, known as libration or Lagrange points. A spacecraft placed at one of these locations can theoretically remain stationary with respect to the two primary bodies, $Earth$ and $Moon$. The libration points $L_1$, $L_2$ and $L_3$ are collinear with the Earth Moon line while the $L_4$ and $L_5$ points form an equilateral triangle with Earth Moon line. $\rho = \frac{M_2}{M_1+M_2}$. For Earth Moon system, $\rho = 0.012151$.

The equations of motion of the spacecraft in the barycenter frame can now be expressed as

$$\ddot{x} - 2\dot{y} - x = -\frac{(1-\rho)(x-\rho)}{r_1^3} - \frac{\rho(x+1-\rho)}{r_2^3} \tag{1}$$

$$\ddot{y} + 2\dot{x} - y = -\frac{(1-\rho)y}{r_1^3} - \frac{\rho y}{r_2^3} \tag{2}$$

$$\ddot{z} = -\frac{(1-\rho)z}{r_1^3} - \frac{\rho z}{r_2^3} \tag{3}$$

where

$$r_1 = \sqrt{(x-\rho)^2 + y^2 + z^2} \tag{4}$$

$$r_2 = \sqrt{(x+1-\rho)^2 + y^2 + z^2} \tag{5}$$

At the equilibrium points, for Z components, the velocity and acceleration relative the two larger bodies are zero. For triangular equilibrium points, the Y component does not equal zero. Solving the above equation, the equilibrium points can be written as $X_{L1} = -0.8369$, $X_{L2} = -1.1560$, $X_{L3} = 1.005$, $X_{L_{4,5}} = \rho - 0.5$ and $Y_{L_{4,5}} = \pm\sqrt{3}/2$ (see Reference 11).

The linearized motion of Equations (1) to (3) and the stability analysis of the L4 points are well studied by Wiesel and Wie (see References 12 and 13). The natural motion about L4 can be conceptualized as the long and short period motions. In the Earth Moon system, the long motions and short motions are 92 and 28 days (see Reference 10).

The general solution for the triangular point orbits can be written as

$$\begin{aligned} x &= A_1 cos(s_1 t) + E_1 sin(s_1 t) + A_2 cos(s_2 t) + E_2 sin(s_2 t) \\ y &= \hat{A}_1 cos(s_1 t) + \hat{E}_1 sin(s_1 t) + \hat{A}_2 cos(s_2 t) + \hat{E}_2 sin(s_2 t) \\ z &= z_0 cos(s_i t) + \frac{\dot{z_0}}{s_i} sin(s_i t) \end{aligned} \tag{6}$$

where $A_{1,2}$, $\hat{A}_{1,2}$, $E_{1,2}$, and $\hat{E}_{1,2}$ are related to the mass parameter $\rho$, the initial states and constants. The parameters $s_1 = 0.297931$, and $s_2 = 0.954587$.

$$\begin{aligned} x_0 &= A_1 + A_2 \\ y_0 &= \hat{A}_1 + \hat{A}_2 \\ \dot{x}_0 &= E_1 s_1 + E_2 s_2 \\ \dot{y}_0 &= \hat{E}_1 s_1 + \hat{E}_2 s_2 \end{aligned} \tag{7}$$

where

$$\begin{aligned} \hat{A}_1 &= \vartheta_i \left[2 s_i E_i - 2.598(\rho - 0.5) A_i\right] \\ \hat{E}_1 &= -\vartheta_i \left[2 s_i A_i + 2.598(\rho - 0.5) E_i\right] \\ \vartheta_i &= 1/{s_i}^2 + 9/4 \end{aligned} \tag{8}$$

The solution to the equations of motion is based on the linearized equations of motion of the CR3BP and therefore is only valid in the vicinity of the associated libration points. In a realistic

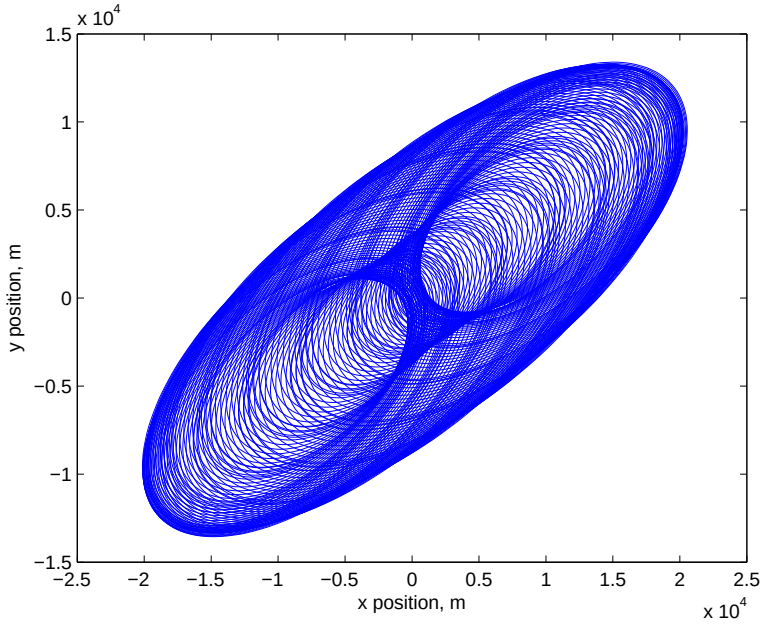


**Figure 2. Trajectory at L4 Short Period Motion 200 Orbits without Solar Gravitation and Without Active Control**

system, the eccentricity and third body perturbations should be taken into account. Also, the perturbations in the trajectory will make the libration point orbits unstable. For station keeping problems, Gomez and Howell considered the multiple shooting station keeping strategy and the reconstruction of a nominal orbit (see References 14 and 15). Lei and Xu used a three order solution to replace Equation 6 and also transformed the station keeping to a nonlinear optimization programming problem (see Reference 16). Zhang and Hou studied the transfer orbits to a short period orbit around the triangular libration points in the Earth Moon System (see Reference 4).

Microsatellites can be launched into an Earth parking orbit with an altitude of about 200 km or 400 km. The drift duration in the parking orbit can be freely chosen, as in the Gaia mission, which allows to select a launch time to minimizing the effort for the insertion manoeuvrings (see Reference 17). Moon gravity assist can be used (see Reference 18). The first part of the maneuver is to transfer the microsatellite from the parking orbit to perilune. The second part is to transfer the microsatellite from the perilune to the nominal orbit. A microsatellite without control is assumed to be placed into L4 short periodic orbit in 200 orbits shown in Figure 2 in this paper. If solar gravitation is be considered, this satellite will follow the trajectory in 200 orbits shown in Figure 3.

## Circular Three Body Problem with Solar Gravitation Modeling

The bicircular four body problem is a simplified version of the circular restricted three body problem with the consideration of solar gravitation and eccentricity (see Reference 19). In this paper, solar gravitation is considered instead of eccentricity. Tapley and Lewallen were the first group to study the Sun's influence on spacecraft motion near the Earth Moon Libration points (see Reference 20). The reference frames used to develop the nonlinear equations of motion are shown in Figure 4 (see Reference 20). The mass of Earth, Moon, Spacecraft and Sun are denoted as $m_1$ , $m_2$, $m_3$ and $m_4$. The distances between Earth, Moon and Sun to the libration point are $r_1$, $r_2$ and

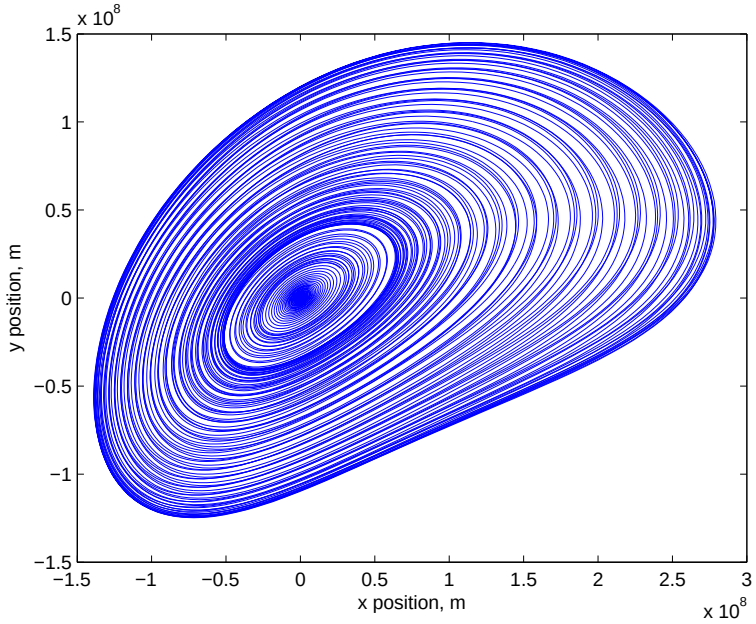


**Figure 3. Trajectory at L4 Short Period Motion 200 Orbits with Solar Gravitation and Without Active Control**

$r_3$. The gravitation constants of Earth, Moon and Sun are denoted as $\mu_1$ , $\mu_2$ and $\mu_3$. The inertial reference frame $I-XYZ$ is located at the the mass centre, or barycenter, of the two primaries. The $X$ axis points towards to the vernal equinox of date. $Y$ lies in the Earth Moon orbit plane. The $Z$ axis points to the direction of the angular velocity vector for the Earth Moon configuration. Also, the $L4$ libration point frame $L_4-\tilde{X}\tilde{Y}\tilde{Z}$ is similar to the $I-XYZ$ frame, except that the origin is shifted to the $L_4$ point. The $\tilde{X}$ axis lies along the Earth Moon line, and $\tilde{Y}$ lies in the Earth Moon Orbit plane. $\tilde{Z}$ coincides with the Z axis. $\Omega$ is the angular velocity of the Earth Moon mass center around the Sun. $R_1$, $R_2$ and $R_3$ are the distances from the Earth, Moon, and Sun to the Earth Moon mass center. $i$ is the inclination of the Earth Moon orbit plane to the ecliptic. $\Psi$ and $\theta$ are the angular positions of the Sun and the Earth Moon Line with respect to the vernal equinox. $\Psi$ is measured in the ecliptic ($\Psi=\Omega t+\Psi_0$). $\Omega=1.99092e-7\ rad/s$. $\theta$ is measured in the Earth Moon orbit plane ($\theta=\omega t+\theta_0$). $\omega=2.665075637e-6\ rad/s$. $\tilde{X}_p$ and $\tilde{Y}_p$ are coordinates of the libration points.

The equations of motion with the Earth, Moon and Sun gravitation forces expressed in the $I-XYZ$ frame, are

$$\begin{aligned}
\ddot{x}-2n\dot{y}-n^2(\tilde{X}_p+x) &= -\frac{\mu_1(\tilde{X}_p+x-R_1)}{r_1^3}-\frac{\mu_2[\tilde{X}_p+x+R_2]}{r_2^3}-\frac{\mu_3[x-x_3]}{r_2^3}-(x_3+\tilde{X}_p)\Omega^2\\
\ddot{y}+2n\dot{x}-n^2(\tilde{Y}_p+y) &= -\frac{\mu_1(\tilde{Y}_p+y)}{r_1^3}-\frac{\mu_2(\tilde{Y}_p+y)}{r_2^3}-\frac{\mu_3(y-y_3)}{r_3^3}-(y_3+\tilde{Y}_p)\Omega^2 \qquad (9)\\
\ddot{z} &= -\frac{\mu_1 z}{r_1^3}-\frac{\mu z}{r_2^3}-\frac{\mu_3(z-z_3)}{r_3^3}-z_3\Omega^2
\end{aligned}$$

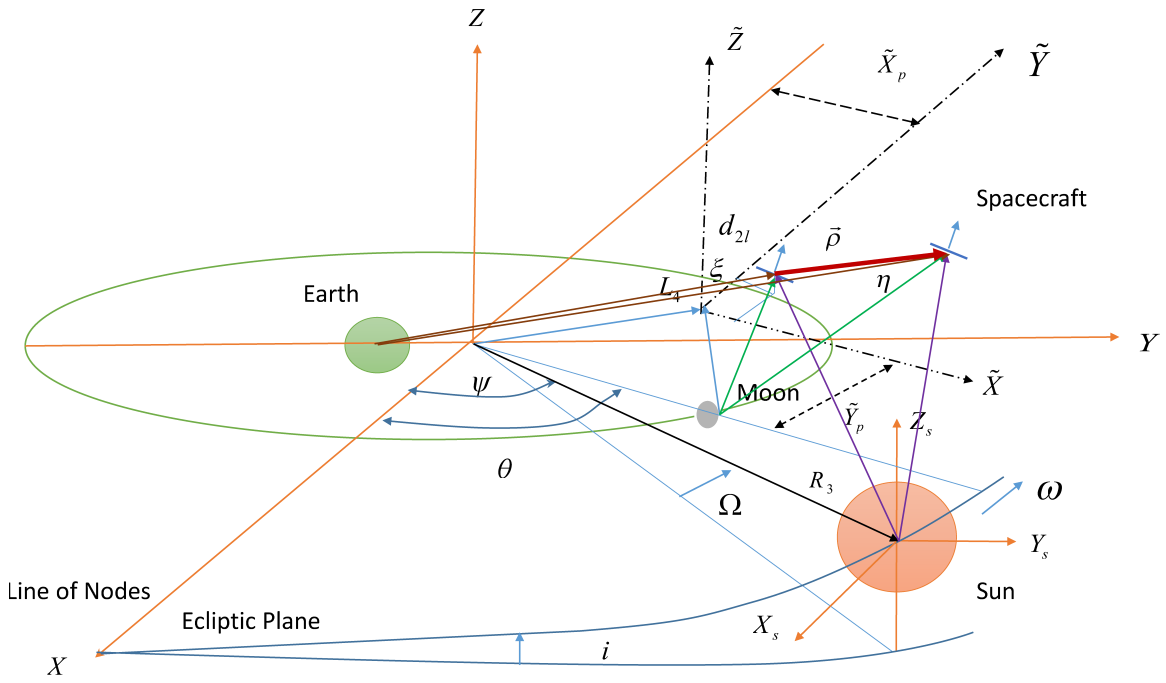


**Figure 4. Three Dimensional Illustration of the Coordinate Systems and Microsatellites Formation Flying Geometry**

where

$$
\begin{aligned}
x_3 &= R_3(cos\Psi con\theta + cosisin\Psi sin\theta) - \tilde{X}_p \\
y_3 &= -R_3(cos\Psi sin\theta - cosisin\Psi sin\theta) - \tilde{Y}_p \\
z_3 &= R_3 sin\Psi sini
\end{aligned} \tag{10}
$$

## SPACECRAFT WITH SOLAR SAIL PROPULSION SYSTEM

The spacecraft propulsion system is responsible for providing thrust. Current L1 and L2 missions usually use a hydrazine fuel based propulsion system. The development of a solar radiation pressure propulsion system has been recently made possible due to advancements in material technology. This innovative technique has the potential to become a viable alternative to chemical propulsion for space mission applications.

### Solar Radiation Pressure Model

Solar Radiation Pressure propulsion is based on Newton's third law (see Reference 21). When light reflects off of a surface, the momentum carried by photons will be transferred to the surface. A perfectly reflective surface can almost double the momentum transfer. Solar Radiation Pressure (SRP) imparts a small amount of force on the sail surface; about $1 \times 10^{-6}\ N/m^2$ at Earth radii. Solar sailing is the concept of using solar radiation pressure to generate useful thrust. In order to harness SRP, solar sails are typically conceived as large area thin films supported by an ultra-lightweight structure. The net solar radiation pressure force is a function of the area of the solar sail and its

orientation. A non-perfectly reflecting solar sail model can be written as

$$\vec{F}_{SRP} = \frac{\beta(1-\rho)}{r_s^2}(\hat{r}_s \cdot \hat{n})\{\rho_{rs}\hat{r}_s + [\rho_{rd}(\hat{r}_s \cdot \hat{n}) + \rho_a]\hat{n}\} \tag{11}$$

The optical parameters for the non-perfectly reflecting behaviour of the solar sail are the reflection coefficient $\rho_s$, the specular reflection factor $s$, the front side $\varepsilon_f$ and back side $\varepsilon_b$ emission coefficients, and the front side $B_f$ and back side $B_b$ non-Lambertian coefficients. $r_s$ is the incoming sun vector. $n$ is the normal vector to the sunline. $\rho_{rs} = \frac{1}{2}(1 - s\rho_s)$. $\rho_{rd} = s\rho_s$. $\rho_a = \frac{1}{2}\left[B_f(1-s)\rho_S + (1-\rho_s)\frac{\varepsilon_f B_f - \varepsilon_b B_b}{\varepsilon_f + \varepsilon_b}\right]$. The solar sail lightness number is

$$\beta = \frac{2p_0}{\mu_s}\frac{A}{m} \tag{12}$$

where $\mu_s$ is the solar gravitational parameter, $A$ is the sail reference area and $m$ is the satellite mass.

The solar radiation pressure model can be written as

$$\vec{f}_{SRP} = (Q_0 + q)(\hat{r}_s \cdot \hat{n})\{\rho_{rs}\hat{r}_s + [\rho_{rd}(\hat{r}_s \cdot \hat{n}) + \rho_a]\hat{n}\} \tag{13}$$

where the solar sail characteristic acceleration is given by

$$Q_0 = \frac{2p_0 A}{m} \tag{14}$$

The variable $q$ is additional control input that represents the variation of the solar sail characteristic acceleration. This is accomplished by varying the solar sail surface area.

The reflectivity, area mass ratio, sail surface and sail orientation can be used as the solar sail control inputs. Typical solar sail designs will be composed of aluminized mylar or Kapton film supported by an underlying lightweight truss. Reference 22 uses an electrochromic material on the solar sail and PID control for L1 artificial Lagrange points mission. This electrochromic material was tested on IKAROS mission (see Reference 23). Mingotti and McInnes also used the electrochromic material for a Femto Spacecraft (see Reference 24). In order to utilize solar radiation pressure force to control a spacecraft, the orientation of the solar sail needs to be continuously changed to generate the required control accelerations (see Reference 25). The constantly changing spacecraft orientation during formation keeping may interfere with mission pointing requirements. The development of the proposed SRP formation control strategy does not require drastic changes to existing libration point spacecraft (Gaia). The solar sail for the microsatellite formation flying at L4 in this paper will use the models in Figures 5 or 7. The proposed sail can use the model in Figure 5. The variable sail reflectivity and sail orientation can be combined for fine control. There are high reflectivity materials which will exploit the solar radiation pressure to produce a propulsive thrust and electrochromic materials which will be used to modulate the thrust without varying the sail attitude (shown in Figure 6). There are also flexible thin film solar cells on the sail which will be used to provide the electric power for the payload and the electrochromic material. Another possibility is to use the model shown in Figure 7 (similar to the model used in Reference 26 which is currently under development at Clyde Space). The advantage of this solar sail is to use the controllable sail surface which is less difficult to control than electrochromic materials. The variable sail surface and sail orientation can be combined for fine control.

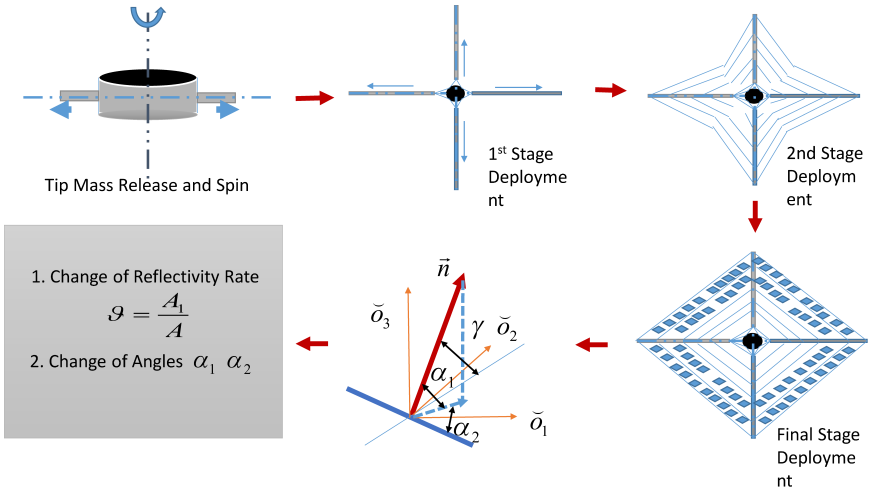


**Figure 5. Flat Solar Sail Propulsion Systems for Microsatellite Formation Flying**

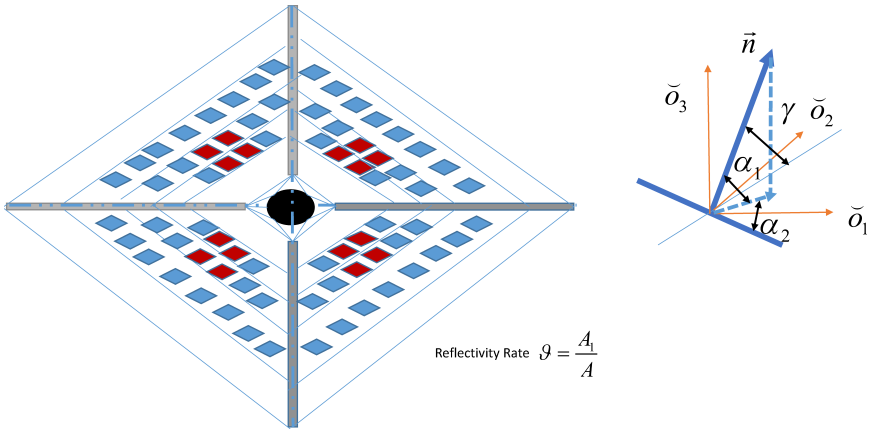


**Figure 6. Solar Sail Model using High Reflectivity Material, Electrochromic Material and Thin Solar Cells**

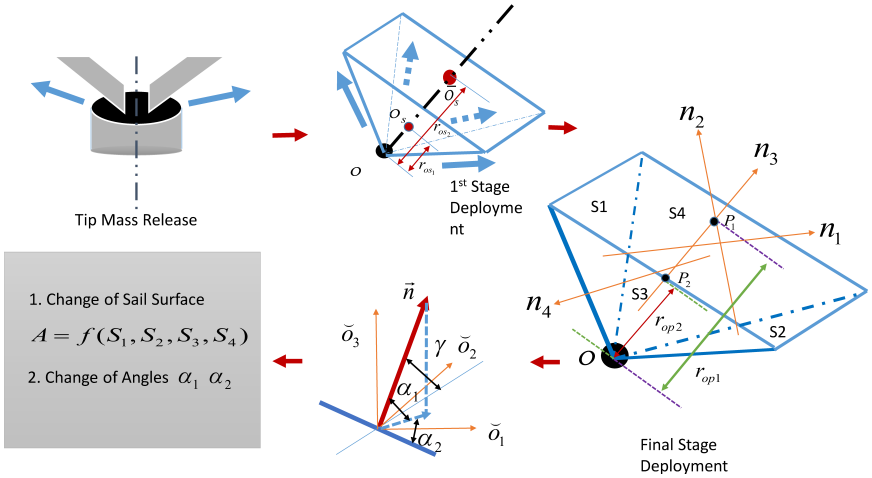


**Figure 7. Four Triangular Sail Propulsion Systems for Microsatellite Formation Flying**

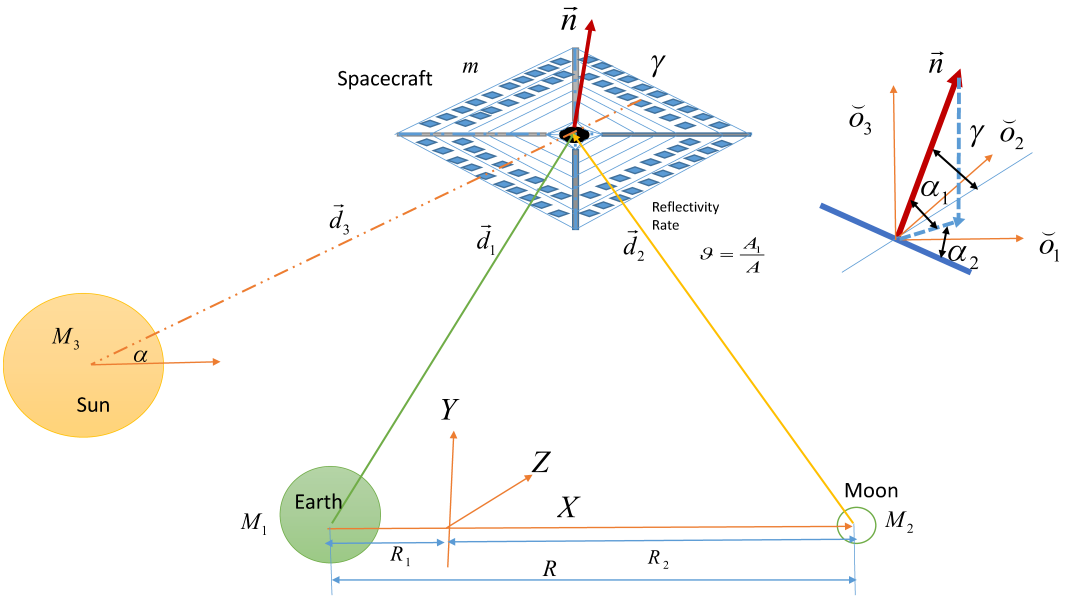


**Figure 8. Microsatellite with Flat Solar Sailing at $L4$ Earth Moon System**

### Solar Radiation Pressure in the Sun/Earth Moon System

In the classical CR3BP there are only five libration points. Using solar radiation pressure, the libration point locations become a function of the sail reflectivity number and orientation. The constant acceleration from a solar sail can be used to generate artificial libration points in the Earth Moon three body problem. This is achieved by directing the thrust due to solar radiation pressure in the anti-sun direction thereby adding to the centripetal force in the rotating Earth Moon frame (see References 25 and 27). Figure 8 show the proposed solar sailing microsatellite at L4 in the Earth Moon System. In Figure 8, $\gamma$ is the angle between $\hat{d}_3$ and $\hat{n}$. $\alpha_1$ and $\alpha_2$ are the pitch and yaw angles of the solar sail. If the sail surface is assumed to be ideal (see References 28 and 29), the solar radiation pressure model Equation (13) can be written as

$$\vec{f}_{SRP} = (\frac{2pA}{m} + q)(\hat{d}_3 \cdot \hat{n})^2 \hat{n} \tag{15}$$

The acceleration of x, y and z can be written as

$$\begin{aligned} x_{SRP} &= (\frac{2pA}{m} + q)\kappa(cos\alpha_1)^3(cos\alpha_2)^3 \\ y_{SRP} &= (\frac{2pA}{m} + q)\kappa(cos\alpha_1)^3(cos\alpha_2)^2 sin\alpha_2 \\ z_{SRP} &= (\frac{2pA}{m} + q)\kappa(cos\alpha_1)^2(cos\alpha_2)^3 sin\alpha_1 \end{aligned} \tag{16}$$

where $\kappa$ includes the inverse square acceleration dependency as the distance from the sun varies (see Reference 29).

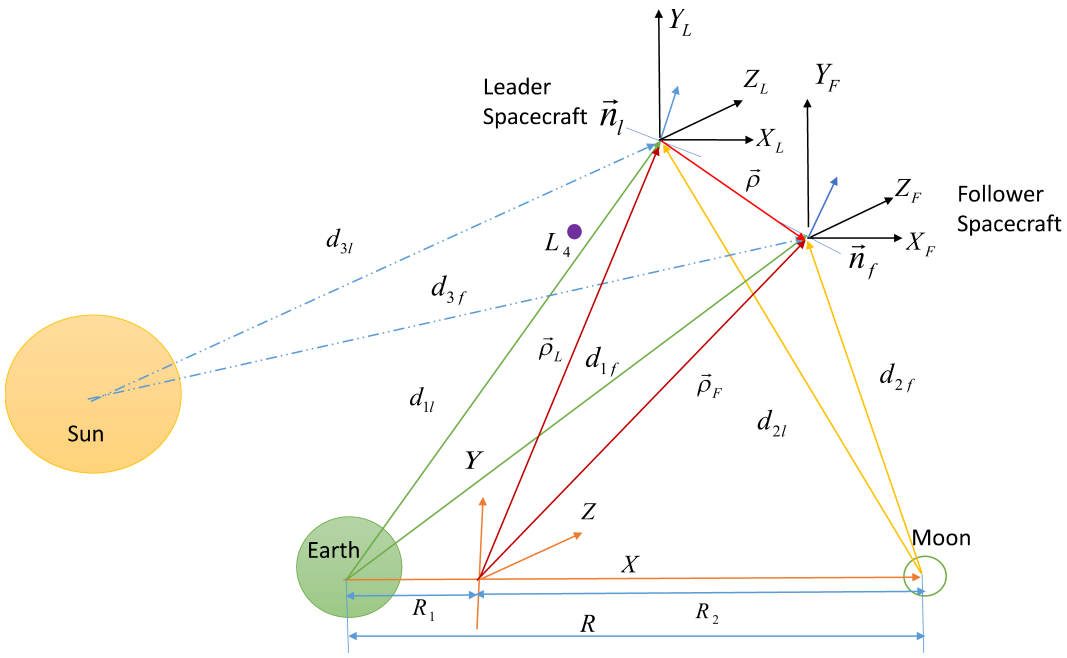


**Figure 9. Schematic Showing the vector Quantities in the Relative Equation of Motion**

## FORMATION FLYING

Many researchers have studied the Libration point formation flying due to the many benefits these missions offer. The success of these missions is tied to the ability of the control system to regulate the trajectory of the formation spacecraft. Follower spacecraft are controlled using solar radiation pressure on a sail and a pulsed plasma thruster. Both the leader and follower spacecraft were assumed identical in solar sail area and mass. The leader spacecraft followed a predetermined unperturbed reference trajectory. Large baseline formations with separation distances of 1 to 25 km were utilized. The equations of motion developed in the previous sections describe the motion of one spacecraft at the Earth Moon $L_4$ point. The follower reference trajectory is specified according to mission objectives.

### Equations of Motion

This section presents the equations of motion of the dynamics of a follower spacecraft relative to a leader spacecraft. The formation dynamics in the CR3BP are formulated using two sets of Equations (9)-(10) for the leader and follower spacecraft (shown in Figure 9). The dynamics of the follower spacecraft relative to the leader satellite is expressed as $\ddot{\vec{\rho}} = \ddot{\vec{\rho}}_F - \ddot{\vec{r}}_L$. Redefining the coordinates $[\ x \quad y \quad z\ ]^T$ as relative coordinates (ie. $x = x_F - x_L$, $y = y_F - y_L$, $z = z_F - z_L$) gives the CR3BP Spacecraft Formation Flying (SFF) equations of motion

$$\ddot{x} - 2\dot{y} - x = -\mu_1 \left[\frac{x}{d_{1F}^3} + [x_1 - x_L]\left(\frac{1}{d_{1F}^3} - \frac{1}{d_{1L}^3}\right)\right] - \mu_2 \left[\frac{x}{d_{2F}^3} + [x_2 - x_L]\left(\frac{1}{d_{2F}^3} - \frac{1}{d_{2L}^3}\right)\right] \tag{17}$$
$$- \mu_3 \left[\frac{x}{d_{3F}^3} + [x_3 - x_L]\left(\frac{1}{d_{3F}^3} - \frac{1}{d_{3L}^3}\right)\right] + f_x$$

$$\ddot{y} + 2\dot{x} - y = -\mu_1 \left[ \frac{y}{d_{1F}^3} + [y_1 - y_L] \left( \frac{1}{d_{1F}^3} - \frac{1}{d_{1L}^3} \right) \right] - \mu_2 \left[ \frac{y}{d_{2F}^3} + [y_2 - y_L] \left( \frac{1}{d_{2F}^3} - \frac{1}{d_{2L}^3} \right) \right] \tag{18}$$
$$- \mu_3 \left[ \frac{y}{d_{3F}^3} + [y_3 - y_L] \left( \frac{1}{d_{3F}^3} - \frac{1}{d_{3L}^3} \right) \right] + f_y$$

$$\ddot{z} = -\mu_1 \left[ \frac{z}{d_{1F}^3} + z_L \left( \frac{1}{d_{1F}^3} - \frac{1}{d_{1L}^3} \right) \right] - \mu_2 \left[ \frac{z}{d_{2F}^3} + z_L \left( \frac{1}{d_{2F}^3} - \frac{1}{d_{2L}^3} \right) \right] \tag{19}$$
$$- \mu_3 \left[ \frac{z}{d_{3F}^3} + [z_3 - z_L] \left( \frac{1}{d_{3F}^3} - \frac{1}{d_{3L}^3} \right) \right] + f_z$$

$f_x$, $f_y$, and $f_z$ are the control inputs provided by $x$, $y$, $z$ thrusters or solar sails. In this paper, Pulsed Plasma Thrusters (PPT) will be installed on the x, y and z axes for SFF (see Reference 30). In order to save fuel, y and z thrusters can be turned off. The x axis PPT thruster and the control of sail pitch and yaw angles will be able to provide the thrust needed for SFF. If the x axis thruster fails, the control of sail area, pitch and yaw angles will be able to provide thrust for SFF. The $x_1$, $x_2$, $y_1$ and $y_2$ are given as

$$\begin{aligned} x_1 &= -(\tilde{X}_p - R_1) \\ x_2 &= -(\tilde{X}_p + R_2) \\ y_1 &= y_2 = -\tilde{Y}_p \end{aligned} \tag{20}$$

The relative distances between the leader and follower spacecraft with respect to Earth, Moon and Sun can be specified

$$\begin{aligned} d_{1L} &= \sqrt{(x_L - x_1)^2 + (y_L - x_1)^2 + {z_L}^2} \\ d_{1F} &= \sqrt{(x_L + x - x_1)^2 + (y_L + y - y_1)^2 + (z_L + z)^2} \\ d_{2L} &= \sqrt{(x_L - x_2)^2 + (y_L - y_2)^2 + (z_L)^2} \\ d_{2F} &= \sqrt{(x_L + x - x_2)^2 + (y_L + y - y_2)^2 + (z_L + z)^2} \\ d_{3L} &= \sqrt{(x_L - x_3)^2 + (y_L - y_3)^2 + (z_L - z_3)^2} \\ d_{3F} &= \sqrt{(x_L + x - x_3)^2 + (y_L + y - y_3)^2 + (z_L + z - z_3)^2} \end{aligned} \tag{21}$$

**Reference Trajectory**

The configuration of the spacecraft formation is directly related to the scientific objectives of the mission. It may be possible to use natural motions as candidate trajectories for some applications in the future, for this future mission study, the trajectories are based on the solution of the linearized equations of motion for SFF in the CR3BP. The leader spacecraft reference motion's period is selected to be equal to that of the short period at L4. The relative reference trajectory can be written based on Equation 6 (see Figure 10).

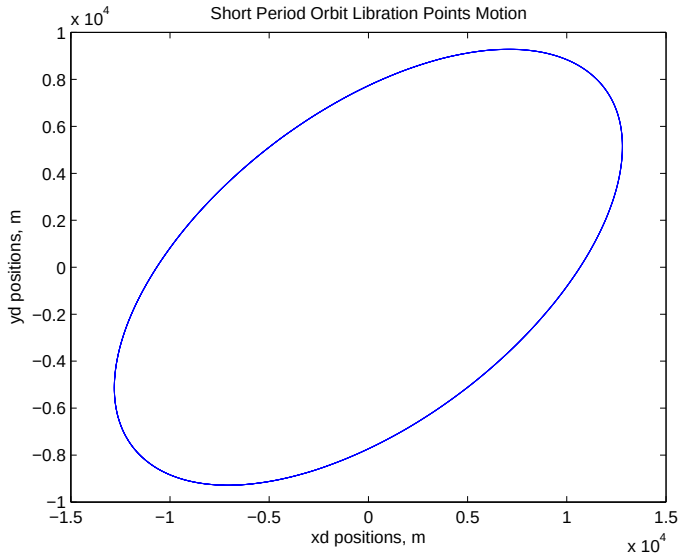


**Figure 10. Leader Reference Trajectory Short Period Motions at Earth Moon L4**

$$x^d = (A_{1F} - A_{1L})cos(s_1 t) + (E_{1F} - E_{1L})sin(s_1 t) + (A_{2F} - A_{2L})cos(s_2 t) + (E_{1F} - E_{1L})sin(s_2 t) \tag{22}$$

$$y^d = (\hat{A}_{1F} - \hat{A}_{1L})cos(s_1 t) + (\hat{E}_{1F} - \hat{E}_{1L})sin(s_1 t) + (\hat{A}_{2F} - \hat{A}_{2L})cos(s_2 t) + (\hat{E}_{2F} - \hat{E}_{2L})sin(s_2 t) \tag{23}$$

$$z^d = (z_{0F} - z_{0L})cos(s_i t) + \frac{(\dot{z}_{0F} - \dot{z}_{0L})}{s_i} sin(s_i t) \tag{24}$$

## DESIGN OF NONAFFINE CONTROL LAWS

The theoretical basis for developing the nonlinear control algorithms for the nonlinear nonaffine mathematical model using solar radiaton pressure is shown in this section(see References 31 and 32). The methods to decompose the original nonaffine system into an affine one in the control part and a nonaffine part representing generalized modeling errors are the mean value theorem, the Taylor series expansion and the contraction mapping method (see References 33, 34 and 35).

It is difficult to invert nonaffine nonlinearities to obtain the inverting control input. Fuzzy logic Systems or neural networks are used to approximate the desired feedback control input (see Reference 36). First, a control method which can account for the nonaffine SRP control inputs is developed. The concept behind this method is to differentiate the nonlinear state equations once so that the resultant augmented equations are linear in $\dot{U}$ and use this as the new control input. Based on the Equations (16)-(19), the lower order states are defined as $\bar{x}_1 \in \mathbb{R}^{6\times 1} = [\ x\ y\ z\ \dot{x}\ \dot{y}\ \dot{z}\ ]^T$, the higher order states $\bar{x}_2 \in \mathbb{R}^{3\times 1} = [\ \ddot{x}\ \ddot{y}\ \ddot{z}\ ]^T$, the full state vector $X \in \mathbb{R}^{9\times 1} = [\ \bar{x}_1\ \bar{x}_2\ ]^T$, and the reference trajectory $X^d \in \mathbb{R}^{9\times 1} = [\ \bar{x}_1^d\ \bar{x}_2^d\ ]^T$. $\dot{\bar{x}_1} \in \mathbb{R}^{6\times 1} = [\ \dot{x}\ \dot{y}\ \dot{z}\ \ddot{x}\ \ddot{y}\ \ddot{z}\ ]^T$. $\dot{\bar{x}_2} \in \mathbb{R}^{3\times 1} = [\ \dddot{x}\ \dddot{y}\ \dddot{z}\ ]^T$.

Using Equations (16)-(19), the nonaffine nonlinear system can be written as

$$\bar{x}_2 = P_1(\bar{x}_2) + G(U) \tag{25}$$

For the purpose of control law development, rewrite nonaffine equations by the mean value theorem and Equation (25) as affine system, so

$$\dot{\bar{x}_2} = \dot{P}_1(\bar{x}_2) + J(U)\dot{U} \tag{26}$$

$$\begin{bmatrix} \dot{\bar{x_1}} \\ \dot{\bar{x}_2} \end{bmatrix} = \begin{bmatrix} \check{A}_{11} & \check{A}_{12} \\ \check{A}_{21} & \check{A}_{22} \end{bmatrix} \begin{bmatrix} \bar{x_1} \\ \bar{x_2} \end{bmatrix} + \begin{bmatrix} \check{B}[P(\bar{x}_2) + G(U) + F_{d1}] \\ \dot{P}(\bar{x}_2) + F_{d2} \end{bmatrix} + \begin{bmatrix} 0_{6\times 3} \\ J(U) \end{bmatrix} \dot{U} \tag{27}$$

where $P(\bar{x_2}) \in \mathbb{R}^{3\times 1}$ is the nonlinear portion of the dynamics, $G(U) \in \mathbb{R}^{3\times 1}$ is the SRP acceleration, $J(U) \in \mathbb{R}^{3\times 1} = \partial G(U)/\partial U$, and $B = [\ 0_{3\times 3}\ I_{3\times 3}\ ]^T$ . Also, the higher and lower order disturbances are $F_{d1} \in \mathbb{R}^{6\times 1}$ and $F_{d2} \in \mathbb{R}^{3\times 1}$ respectively.

The nonlinear term $P(\bar{x_2})$ represents the gravitational acceleration due to the Earth, Moon and Sun.

$$P(\bar{x_2}) = \begin{bmatrix} -\mu_1 P_{11} - \mu_2 P_{12} - \mu_3 P_{13} \\ -\mu_1 P_{21} - \mu_2 P_{22} - \mu_3 P_{23} \\ -\mu_1 P_{31} - \mu_2 P_{32} - \mu_3 P_{33} \end{bmatrix}$$

$$\begin{aligned} P_{11} = & \frac{x}{((x_L + x - x_1)^2 + (y_L + y - y_1)^2 + (z_L + z)^2)^{3/2}} \\ & + [x_1 - x_L]\frac{1}{((x_L + x - x_1)^2 + (y_L + y - y_1)^2 + (z_L + z)^2)^{3/2}} \\ & - [x_1 - x_L]\frac{1}{((x_L - x_1)^2 + (y_L - x_1)^2 + {z_L}^2)^{3/2}} \end{aligned} \tag{28}$$

$$\begin{aligned} P_{12} = & \frac{x}{((x_L + x - x_2)^2 + (y_L + y - y_2)^2 + (z_L + z)^2)^{3/2}} \\ & + [x_2 - x_L]\frac{1}{((x_L + x - x_2)^2 + (y_L + y - y_2)^2 + (z_L + z)^2)^{3/2}} \\ & - [x_2 - x_L]\frac{1}{((x_L - x_2)^2 + (y_L - y_2)^2 + (z_L)^2)^{3/2}} \end{aligned} \tag{29}$$

$$\begin{aligned} P_{13} = & \frac{x}{((x_L + x - x_3)^2 + (y_L + y - y_3)^2 + (z_L + z - z_3)^2)^{3/2}} \\ & + [x_3 - x_L]\frac{1}{((x_L + x - x_3)^2 + (y_L + y - y_3)^2 + (z_L + z - z_3)^2)^{3/2}} \\ & - [x_3 - x_L]\frac{1}{((x_L - x_3)^2 + (y_L - y_3)^2 + (z_L - z_3)^2)^{3/2}} \end{aligned} \tag{30}$$

$$P_{21} = \frac{y}{((x_L + x - x_1)^2 + (y_L + y - y_1)^2 + (z_L + z)^2)^{3/2}} + [y_1 - y_L]\frac{1}{((x_L + x - x_1)^2 + (y_L + y - y_1)^2 + (z_L + z)^2)^{3/2}} - [y_1 - y_L]\frac{1}{((x_L - x_1)^2 + (y_L - x_1)^2 + {z_L}^2)^{3/2}} \tag{31}$$

$$P_{22} = \frac{y}{((x_L + x - x_2)^2 + (y_L + y - y_2)^2 + (z_L + z)^2)^{3/2}} + [y_2 - y_L]\frac{1}{((x_L + x - x_2)^2 + (y_L + y - y_2)^2 + (z_L + z)^2)^{3/2}} - [y_2 - y_L]\frac{1}{((x_L - x_2)^2 + (y_L - y_2)^2 + (z_L)^2)^{3/2}} \tag{32}$$

$$P_{23} = \frac{y}{((x_L + x - x_3)^2 + (y_L + y - y_3)^2 + (z_L + z - z_3)^2)^{3/2}} + [y_3 - y_L]\frac{1}{((x_L + x - x_3)^2 + (y_L + y - y_3)^2 + (z_L + z - z_3)^2)^{3/2}} - [y_3 - y_L]\frac{1}{((x_L - x_3)^2 + (y_L - y_3)^2 + (z_L - z_3)^2)^{3/2}} \tag{33}$$

$$P_{31} = \frac{z}{((x_L + x - x_1)^2 + (y_L + y - y_1)^2 + (z_L + z)^2)^{3/2}} + z_L\frac{1}{((x_L + x - x_1)^2 + (y_L + y - y_1)^2 + (z_L + z)^2)^{3/2}} - z_L\frac{1}{((x_L - x_1)^2 + (y_L - x_1)^2 + {z_L}^2)^{3/2}} \tag{34}$$

$$P_{32} = \frac{z}{((x_L + x - x_2)^2 + (y_L + y - y_2)^2 + (z_L + z)^2)^{3/2}} + z_L\frac{1}{((x_L + x - x_2)^2 + (y_L + y - y_2)^2 + (z_L + z)^2)^{3/2}} - z_L\frac{1}{((x_L - x_2)^2 + (y_L - y_2)^2 + (z_L)^2)^{3/2}} \tag{35}$$

$$P_{33} = \frac{z}{((x_L + x - x_3)^2 + (y_L + y - y_3)^2 + (z_L + z - z_3)^2)^{3/2}} + [z_3 - z_L]\frac{1}{((x_L + x - x_3)^2 + (y_L + y - y_3)^2 + (z_L + z - z_3)^2)^{3/2}} - [z_3 - z_L]\frac{1}{((x_L - x_3)^2 + (y_L - y_3)^2 + (z_L - z_3)^2)^{3/2}} \tag{36}$$

$$G(U) = \begin{bmatrix} (\frac{2pA}{m} + q)\kappa(cos\alpha_1)^3(cos\alpha_2)^3 \\ (\frac{2pA}{m} + q)\kappa(cos\alpha_1)^3(cos\alpha_2)^2 sin\alpha_2 \\ (\frac{2pA}{m} + q)\kappa(cos\alpha_1)^2(cos\alpha_2)^3 sin\alpha_1 \end{bmatrix} \tag{37}$$

where $\check{A}_{11} = 0_{3\times3}$ and $\check{A}_{12} = I_{3\times3}$.

$$\check{A}_{21} = \begin{bmatrix} 1 & 0 & 0 \\ 0 & 1 & 0 \\ 0 & 0 & 0 \end{bmatrix} \tag{38}$$

$$\check{A}_{22} = \begin{bmatrix} 0 & 2 & 0 \\ -2 & 0 & 0 \\ 0 & 0 & 0 \end{bmatrix} \tag{39}$$

$$\check{B} = \begin{bmatrix} 0_{3\times3} \\ I_{3\times3} \end{bmatrix} \tag{40}$$

Note that the control input $U \in \mathbb{R}^{3\times1} = [\ q\ \phi\ \alpha\ ]^T$ does not appear linearly in Equations (17-19). To develop a control law for this system, the order of the system is increased and $\dot{U}$ is used as the actual control input. The desired reference trajectory $X^d \in \mathbb{R}^{9\times1}$ can be expressed as

$$\begin{bmatrix} \dot{\bar{x}}_1^d \\ \dot{\bar{x}}_2^d \end{bmatrix} = \begin{bmatrix} \check{A}_{11}^d & \check{A}_{12}^d \\ \check{A}_{21}^d & \check{A}_{22}^d \end{bmatrix} \begin{bmatrix} \bar{x_1}^d \\ \bar{x_2}^d \end{bmatrix} \tag{41}$$

The error dynamics of the system can be formulated using Equations (27) and (41) as

$$\begin{bmatrix} \dot{S} \\ \ddot{S} \end{bmatrix} = \begin{bmatrix} \check{A}_{11} & \check{A}_{12} \\ \check{A}_{21} & \check{A}_{22} \end{bmatrix} \begin{bmatrix} S \\ \dot{S} \end{bmatrix} + \begin{bmatrix} 0 \\ \bar{\check{A}}_{21}\bar{x_1}^d + \bar{\check{A}}_{22}\bar{x_2}^d \end{bmatrix} + \begin{bmatrix} \check{B}[P(\bar{x_2}) + G(U)] \\ \dot{P}(\bar{x_2}) \end{bmatrix} + \begin{bmatrix} 0_{6\times3} \\ J(U) \end{bmatrix} \dot{U} \tag{42}$$

where $\bar{\check{A}}_{21} = \check{A}_{21} - \check{A}_{21}^d$ and $\bar{\check{A}}_{22} = \check{A}_{22} - \check{A}_{22}^d$. The tracking error $e \in \mathbb{R}^{6\times1} = X - X^d$ is composed of the lower order tracking error ($S = \dot{e} + \bar{K}e$) and the higher order tracking error $\dot{S}$.

$$\bar{K} = \begin{bmatrix} k_1 & 0 & 0 & k_4 & 0 & 0 \\ 0 & k_2 & 0 & 0 & k_5 & 0 \\ 0 & 0 & k_3 & 0 & 0 & k_6 \end{bmatrix} \tag{43}$$

**Nonaffine system using Solar Sail**

The control law using solar sails were developed where all three control inputs $U = [\ q\ \phi\ \alpha\ ]^T$ are available. The error dynamics for this case are expressed as Equation (42).

To complete the control design, a description of possible disturbances is included. The disturbance is assumed to be unknown and bounded. The sliding manifold can be written

$$\sigma \in \mathbb{R}^{3\times 1} = \dot{S} + \hat{K}S \tag{44}$$

where $\dot{\sigma} = \ddot{S} + \hat{K}\dot{S}$.

The Jacobian for this case is

$$J(U) = \begin{bmatrix} c_{\alpha_1}^3 c_{\alpha_2}^3 & -3(\frac{2pA}{m}+q)\kappa c_{\alpha_1}^3 c_{\alpha_2}^2 s_{\alpha_2} & -3(\frac{2pA}{m}+q)\kappa c_{\alpha_1}^2 c_{\alpha_2}^3 s_{\alpha_1} \\ c_{\alpha_1}^3 c_{\alpha_2}^2 s_{\alpha_2} & (\frac{2pA}{m}+q)\kappa(-2c_{\alpha_1}^3 c_{\alpha_2} s_{\alpha_2}^2 + c_{\alpha_1}^3 c_{\alpha_2}^3) & -3(\frac{2pA}{m}+q)\kappa c_{\alpha_1}^2 c_{\alpha_2}^2 s_{\alpha_2} s_{\alpha_1} \\ c_{\alpha_1}^2 c_{\alpha_2}^2 s_{\alpha_1} & -2(\frac{2pA}{m}+q)\kappa c_{\alpha_1}^2 c_{\alpha_2} s_{\alpha_1} s_{\alpha_2} & (\frac{2pA}{m}+q)\kappa(-2c_{\alpha_1} c_{\alpha_2}^2 s_{\alpha_1}^2 + c_{\alpha_1}^3 c_{\alpha_2}^2) \end{bmatrix} \tag{45}$$

The control law is

$$\dot{U} = \begin{bmatrix} \dot{q} \\ \dot{\phi} \\ \dot{\alpha} \end{bmatrix} = -J(U)^{-1}\left[\eta\sigma + \hat{K}\dot{S} + \check{A}_{21}\bar{x_1} + \check{A}_{22}\bar{x_2} + \dot{P}(\bar{x}_2) - \dot{\bar{x}_2}^d\right] \tag{46}$$

where $\eta$ is a positive definite gain matrix

$$\eta = \begin{bmatrix} \eta_x & 0 & 0 \\ 0 & \eta_y & 0 \\ 0 & 0 & \eta_z \end{bmatrix} \tag{47}$$

If $F_{d1}$ and $F_{d2}$ are not zero, the use of the above control law will not be able to provide good performance. The function $\dot{P}(\bar{x}_2) + F_{d2}$ can be replaced with the function $\bar{P}(\bar{x}_2)$. The fuzzy logic system was chosen due to its universal approximation property. For an input vector $X$, which is constructed of the measured states, the reference model outputs and the pseudo-control signal, the output of the fuzzy logic system, is given by

$$\bar{P}(X) = W^T\zeta \tag{48}$$

where $W$ is the output weighting matrix. The optimal output weighting can be given by

$$W^* = arg\underset{W\in\bar{\varpi}_P}{min}\underset{X\in D_x}{sup}\left|\hat{P} - \bar{P}\right| \tag{49}$$

The weighting function can be written as

$$\dot{W} = \beta\zeta\sigma \tag{50}$$

$\zeta$ is a vector of sigmoid activation functions. The $N$ Gaussian membership functions are $\mu_{Wi}(\sigma_i)$ $(i = 1 - N)$.

$$\zeta = \frac{\prod_{i=1}^{N} \mu_{Wi}(\sigma_i)}{\sum_{l=1}^{P} \prod_{i=1}^{N} \mu_{Wi}(\sigma_i)} \tag{51}$$

$$\hat{P} - \bar{P}(W^*) = \varpi_P \tag{52}$$

where $\varpi_P$ is the approximation error and bounded in the compact set $U_x$. $\left\|\varpi_P\right\| \leq \bar{\varpi}_P$. Approximation errors can be reduced by increasing the number of fuzzy rules.

The control law can be rewritten as

$$\dot{U} = \begin{bmatrix} \dot{q} \\ \dot{\phi} \\ \dot{\alpha} \end{bmatrix} = -J(U)^{-1} \left[ \eta\sigma + \hat{K}\dot{S} + \check{A}_{21}\bar{x_1} + \check{A}_{22}\bar{x_2} + W^T\zeta - \dot{\bar{x_2}}^d \right] \tag{53}$$

**Stability Analysis**

In this section, the stability of the control law using solar sails will be analyzed.

**Theorem 1:** For the system model in Equation (27), if the weighted tracking error is specified as Equations (44) and (43), and the SRP control law is specified as Equations (50) and (53), then the system tracking error $e(t)$ will converge to zero.

**Proof:** $\bar{W}$ to represent the fuzzy parameter errors is defined, where $\bar{W} = W^* - W$. $\dot{\bar{W}} = \dot{W}^* - \dot{W}$. In order to establish the stability of the control laws, the candidate Lyapunov function is considered

$$V(S) = \frac{1}{2}\sigma^T\sigma + \frac{1}{2\beta}\bar{W}^T\bar{W} \tag{54}$$

and it's corresponding derivative is

$$\begin{aligned} \dot{V}(S) &= \sigma^T\dot{\sigma} + \frac{1}{\beta}\bar{W}^T\dot{\bar{W}} \\ &= \sigma^T \left[ \hat{K}\dot{S} + \ddot{S} \right] + \frac{1}{\beta}\bar{W}^T\dot{\bar{W}} \\ &= \sigma^T \left[ \hat{K}\dot{S} + \check{A}_{21}\bar{x_1} + \check{A}_{22}\bar{x_2} + \dot{P}(X) + J(U)\dot{U} + \dot{\bar{x_2}}^d \right] + \frac{1}{\beta}\bar{W}^T\dot{\bar{W}} \end{aligned} \tag{55}$$

We can use the adaptive control law Equation (50) and the control law Equation (53):

$$\dot{V}(\sigma) = -\sigma^T\eta\sigma + \bar{\varpi}_P \tag{56}$$

which is negative definite. This indicates that $V$ is a non-increasing Lyapunov function in $\sigma$-space.

This implies that as $t \to \infty$, $V(t) = V_\infty$. Thus $\sigma \in \mathfrak{L}_\infty$. Defining $\lambda_{min}(\eta)$ can be established that as the minimum eigenvalue of the positive definite matrix $\eta$.

$$\dot{V} \leq -\lambda_{min}(\eta)\|\sigma\|^2 + \bar{\varpi}_P \tag{57}$$

Similar to Theorem 1, $\sigma \in \mathfrak{L}_2$ is obtained. $\dot{\sigma} \in \mathfrak{L}_\infty$ and $\sigma \in \mathfrak{L}_2 \bigcap \mathfrak{L}_\infty$ is deduced. Using Barbalat's lemma, it can be shown that $\sigma \to 0$ as $t \to \infty$. Therefore, control law as specified by Equation (53) ensures asymptotic convergence of the position and velocity tracking errors.

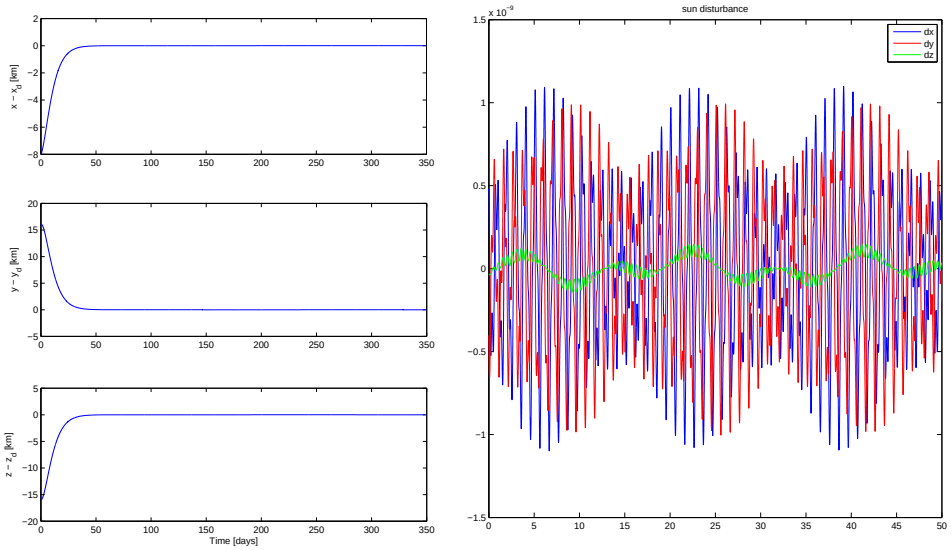


**Figure 11. Simulation Results with the Proposed Control Algorithm**

## RESULTS

To study the effectiveness of the developed SRP formation keeping control laws, the control inputs of Equation (53), and the reference trajectories are numerically simulated using the full nonlinear model. The system parameters used in this study are listed in Table 1.

**Table 1. Reference System Parameters**

| Parameter | Value |
|---|---|
| $A$ | 150 [m$^2$] |
| $m_1$ | $5.98 \times 10^{24}$ [kg] |
| $m_2$ | $7.35 \times 10^{22}$[kg] |
| $m_3$ | $1.99 \times 10^{30}$[kg] |
| $m_4$ | 50 [kg] |
| $\mu_1$ | 0.987891 |
| $\mu_2$ | 0.012151 |
| $\mu_3$ | 328900.48 |
| $\rho_s, s, \varepsilon_f, \varepsilon_b, B_f, B_b$ | $0.88, 0.94, 0.05, 0.55, 0.79, 0.55$ |

The control angles are subject to the conditions $|\alpha_1| < \pi/2$ and $|\alpha_2| < \pi/2$. The performance of the proposed SRP $L_4$ formation keeping control strategy is examined (shown in Figure 11).

## SUMMARY

Microsatellite formation flying mission located in the vicinity of the $L_4$ libration point was studied. The system was comprised of a leader and follower spacecraft using Pulsed Plasma Thrusters and Solar Sails. CR3BP equations were used along with a solar gravitation model. A proposed nonaffine controller was developed based on the nonlinear equations of motion to account for the nonaffine structure of the solar radiation pressure model control inputs. A control law that drives

the system states to the sliding manifold thereby forcing the plant to follow the desired reference trajectory was then formulated based on Lyapunov theory. Numerical results show that the proposed control method was able to maintain the desired formation.

## REFERENCES


[1] Gomez, G., Masdemont. J., Modelo. J. M., "Libration Points: a Survey from the Dynamical Point of View", Proceedings of the Conference on Libration Point Orbits and Applications, Spain, 2002.

[2] Gomez, G., Llibre, J., Martinez, R., Simo, C., "Dynamics and Mission Design near Libration Point Orbits", Vol. II, Fundamentals: The case of Triangular Libration Points, World Scientific, Singapore, 2001.

[3] Shirobokov, M. G., "Libration Points Orbits and Manifolds: Design and Station Keeping", Keldysh Institude Prepints, No. 90, 2014.

[4] Zhang, Z. T. and Hou, X. Y., "Transfer Orbits to the Earth Moon Triangular Libration Points", Advances in Space Research, Vol. 99, No. 99, 2015.

[5] Schutz, B. F., "Orbital Mechanics of Space Colonies at L4 and L5 of the Earth Moon System", Aerospace Sciences Meeting, 15, 1977, Los Angeles, California, No. 77-33.

[6] Catlin, K. A. and McLaughlin, C. A., "Earth Moon Triangular Libration Point Spacecraft Formations", Journal of Spacecraft and Rockets, Vol. 44, No. 3, 2007, pp 660-670.

[7] Funase, R., Nakasuka, S., Kawakatsu, Y., Fukushima, Y., Tomiki, A., Kodayashi, Y., Nakatsuka, J. and Mita, M., "50 Kg Class Deep Space Exploration Technology Demonstration Microspacecraft PROCYON", 28th Annual AIAA/USU Small Satellite, SSC14-vi-3, Utah, 2014.

[8] Bando, M. and Ichikawa, A., "Formation Flying Along Halo Orbit of Circular Restricted Three Body Problem", Journal of Guidance Control and Dynamics, Vol. 38, No. 1, 2015, pp 123-129.

[9] Gurfil, P., Idan, M., Kasdin, N. J., "Adaptive Neural Control of Deep Space Formation Flying", Journal of Guidance Control and Dynamics, Vol. 26, No. 3. 2003, pp 491-501.

[10] Szebehely, V., "Theory of Orbits: The restricted Problem of Three Bodies", Acdamic Press, New York, 1967.

[11] Curtis, H.D, "Orbital Mechanics for Engineering Students", Elsevier Butterworth Heinemann, Oxford, 2005.

[12] Wiesel, W. E., "Spaceflight Dynamics", McGraw-Hill, New York, 1989.

[13] Wie, B., "Space Vehicle Dynamics and Control", AIAA Publications, Virginia, 1998.

[14] Gomez, G., Masdemont, J., and Simo, C., "Quasihalo Orbits Associated with Libration Points", Journal of the Astronautical Sciences, 1998, Vol 46, No. 2, pp 135-176.

[15] Howell, K. C. and Pemicka, H. J., "Numerical Determination of Lissajous Trajectories in the Restricted Three Body Problem", Celestial Mechanics, 1987, Vol 41, pp 107-124.

[16] Lei, H. L. and Xu. B., "High Order Analytical Solutions around Triangular libration Points in the Circular Restricted Three Body Problem", Monthly Notices of the Royal Astronimical Society, 2013, Vol. 434, No. 2, pp 1376-1386.

[17] Renk, F. and Landgraf, M., "GAIA: Trajectory Design with Tightening Constraints", 24th International Symposium on Space Flight Dynamics, Laurel, Maryland, May 5-9, 2014.

[18] Salazar F. J. T., Macau, E. E. N., and Winter, O. C., "Alternative Transfer to the Earth Moon Lagrangian Points L4 and L5 using Lunar Gravity Assist", Advances in Space Research, Vol. 53, 2014, pp 543-557.

[19] Salazar F. J. T., Winter, O. C., Macau, E. E. N., Masdemont, J., Gomez, G., "Natural Configurations for Formation Flying Around Triangular Libration Points for the Elliptic and the Bicircular Problem in the Earth-Moon System", 65th International Astronautical Congress, Toronto, Canada, IAC-14-C1.1.13. 25737, 2014.

[20] Tapley, B. D., Lewallen, J. M., "Solar Influence on Satellite Motion near the Stable Earth Moon Libration Points", AIAA Journal, Vol. 2, No. 4, 1963, pp 728-732.

[21] McInnes C. R., "Solar Sailing: Technology, Dynamics and Mission Applications", Springer Praxis, London, 1999.

[22] Aliasi, G., Mengali, G., "Artifical Lagrange Points for Solar Sail with Electrochromic Material Panels", Journal of Guidance, Control and Dynamics, Vol. 36., No. 5., 2013, pp 1544-1550.

[23] Funase, R., Shirasawa, Y., Mimasu, Y., Mori, O., Tsuda, Y., Saiki, T., and Kawaguchi, J., "Fuel Free and Oscillation Free Attitude Control of IKAROS Solar Sail Spacecraft using Reflectivity Control Device", 28th International Symposium on Space Technology and Science, 2011.

[24] Mingotti, G. and McInnes, C., "Reconfiguration Manevers for Swarm of High Area to Mass Ratio Spacecraft", 24th International Symposium on Space Flight Dynaimcs, Laurel, Maryland, May 5-9, 2014.

[25] Shahid, K. and Kumar, K. D, "Formation Control at the Sun Earth L2 Libraion Point Using Solar Radiation Pressure", Journal of Spacecraft and Rockets, Vol. 47, No. 4, 2010, pp 614-626.

[26] Ceriotti, M., Harkness, P. and McRobb, M., "Variable Geometry Solar Sailing: The Possibilities of the Quasi Rhombic Pyramid", Advances in Solar Sailing, Springer Praxis Books, Berlin, 2014, pp 899-919.

[27] Gong, S. P., Li, J. F. and Simo, J., "Orbital Motions of a Solar Sail Around the L2 Earth Moon Libration Point", Journal of Guidance, Control, Dynamics, Vol. 37, No. 4, 2014, pp 1349-1356.

[28] Simo. J. and McInnes, C. R., "Displaced Solar Sail Orbits: Dynamics and Applications", 20th AAS/AIAA Space Flight Mechanics Meeting, Feb 14-17 2010, San Diego, California.

[29] Bookless, J. and McInnes, C., "Dynamics and Control of Displaced Periodic Orbits using Solar Sail Propulsion", Journal of Guidance, Control and Dynamics, Vol. 29, No. 3, 2006, pp 527-537.

[30] Wir, B., Murphy, D., Paluszek, M., and Thomas, S., "Robust Attitude Control Systems Design for Solar Sails, Part 2: MicroPPT based Secondary ACS", AIAA Guidance, Navigation and Control Conference and Exhibit, AIAA 2004-5011, Providence, Rhode Island.

[31] Boskovic, J. D., Chen, L. J. and Mehra, R. K., "Adaptive Control Design for Nonaffine Models Arising in Flight Control", Journal of Guidance, Control and Dynamics, Vol. 27, No. 2, 2004, pp 209-217.

[32] Gao, D. X., Lu, D. M. and Sun, Z. Q., "Fuzzy Adaptive Control for a Class of Non-affine Systems via Time Scale Separation", Proceedings of the World Congress on Engineering and Computer Science 2012, Vol II WCECS 2012, October 24-26, 2012, San Francisco, USA.

[33] Labiod, S. and Guerra, T. M., "Adaptive Fuzzy Control of a Class of SISO Nonaffine Nonlinear Systems", Fuzzy Sets and Systems, Vol. 158, 2007, pp 1126-1137.

[34] Leu, Y. G., Wang, W. Y., Lee, T. T., "Observer based Direct Adapive Fuzzy Neural Control for Nonaffine Nonlinear Systems", IEEE Transactionos on Neural Networks, Vol. 5, No. 4, 2005, pp 853-861.

[35] Park, J. H., Hun, S. H., Kim, S. H., Seo, S. J., and Park, G. T., "Direct Adaptive Controller for Nonaffine Nonlinear Systems using Self Structuring Networks", IEEE Transactions on Neural Networks, Vol. 16, No. 2, 2005, pp 414-422.

[36] Park, J. -H., Park, G. -T., Kim, S. -H., Moon, C.-J., "Direct Adaptive Self Structuring Fuzzy Controller for Nonaffine Nonlinear System", Fuzzy Sets and Systems, Vol. 153, 2005, pp 429-445.